Journal of Magnetic Resonance 308 (2019) 106592

Contents lists available at ScienceDirect

Journal of Magnetic Resonance

journal homepage: www.elsevier.com/locate/jmr

A two-region transport model for interpreting T_1-T_2 measurements in complex systems

James E. Maneval [a], Madison L. Nelson [b], Linn W. Thrane [c], Sarah L. Codd [c], Joseph D. Seymour [d,*]

[a] Department of Chemical Engineering, Bucknell University, Lewisburg, PA, USA
[b] Department of Physics, Montana State University, USA
[c] Department of Mechanical and Industrial Engineering, Montana State University, USA
[d] Department of Chemical and Biological Engineering, Montana State University, Bozeman, MT, USA

ARTICLE INFO

Article history:
Received 9 July 2019
Revised 5 September 2019
Accepted 5 September 2019
Available online 6 September 2019

Keywords:
T_1-T_2 relaxation correlation
Diffusive coupling
Two-pore model
Time domain signal

ABSTRACT

A 1D two region coupled pore model with discrete pore coupling is developed to elucidate the eigenmode interactions in regions with different surface relaxivity. Numerical solution of the model and simulation of the correlation experiment for varying surface relaxivity, pore connectivity and pore size ratio indicate the role of negative eigenmodes and overlap of T_1 and T_2 eigenmodes in generating a time domain signal increase with inversion recovery time, t_1. The eigenmodes and eigenfunctions are considered in detail providing connection between the mathematical model and the diffusion dynamics and spin physics of the system. Physical systems, *i.e.* a microporous glass bead pack, a cyclopentane/water hydrate former, and beeswax, showing experimentally measured T_1-T_2 time domain signal rise are considered within the limitations of the model.

1. Introduction

Transverse (spin-spin) and longitudinal (spin-lattice) relaxation have long been known to depend on pore size and surface proportions in porous media [1] and material properties such as molecular density and viscosity [2]. Restrictions in rotational and translational diffusion due to the physicochemical environment of the spin-bearing molecules generate variations in relaxation process that lead to important effects in observed relaxation behavior. Multi-dimensional relaxation methods provide the means to study the coupling of T_1 and T_2 relaxation mechanisms, or modes, through T_1-T_2 correlation experiments and the interplay of T_2-T_2 correlations over a T_1 storage time [3–5]. A complicating aspect of such measurements is the inversion of the time-domain data from an experiment by a regularized Fredholm integral method i.e. inverse Laplace transform (ILT) [6], or other nonlinear inversion method. The presence of negative eigenmodes in the spectral form of the data and the implications of these types of modes for inversion stability in such spectra has been broadly discussed [7–10].

Analysis of T_1-T_2 correlation and T_2-T_2 exchange experiments by direct use of the time-domain voltage signals provides a route to avoiding the artifacts due to data inversion [8,9,11]. The interpretation of exchange phenomena in the time domain of T_2-T_2 experiments indicate signal curvature, a *cosh* modulation, due to exchange dynamics between two T_2 populations [11]. In T_1-T_2 experiments, Song et al. [8] have demonstrated an increase in signal amplitude with inversion recovery time, t_1 for different echo times $t_2 = n\tau$ due to coupling of pore spin dynamics in a two-pore porous media and discussed the effect in terms of negative eigenmodes in the T_1-T_2 spectra. In this paper, the eigenfunction solution framework of Song et al. [12] is further developed to explore a coupled pore system and understand anomalous observed voltage signal increases in T_1-T_2 experiments by time-domain analysis. It is found that negative eigenvalue modes are a necessary, but not sufficient condition, for the signal increase.

The motivation for the development in this paper is two-fold. First, the model, which explicitly couples the pores through magnetization conservation and exchange [13,14], provides enhanced understanding of the T_1-T_2 experiment for the characterization of classical multiscale porous media [15]. Second, the model and its solution can provide routes to interpretation of molecular dynamics in reacting and soft matter systems in which such signal increases have been observed. Specifically, in addition to the first observations of signal rises in the T_1-T_2 signal [7], signal-rise results have been observed in a model hydrate forming system [16], a polymer-solvent system undergoing a glass or gel transition [17] and waxes undergoing solid-solid rotator phase transitions

* Corresponding author at: 306 Cobleigh Hall, Chemical and Biological Engineering, Montana State University, Bozeman, MT 59717-3920, USA.
E-mail address: jseymour@montana.edu (J.D. Seymour).

https://doi.org/10.1016/j.jmr.2019.106592
1090-7807/

[18]. In order to develop a solid basis for interpretation in this wide range of systems, the model is analyzed over a range of parameters related to pore- or population-size ratio, pore connectivity or exchange between pores, and the relaxation modes specific to each pore type. The analysis allows identification of regions of parameter space for which the increase in signal with experimental inversion recovery time t_1 is predicted, demonstrating that the coupling of the T_1- and T_2-relaxation modes in individual pores can be probed by the T_1-T_2 experiment. The relaxation modes are coupled in terms of whether they are in the fast or slow diffusion limit [19].

In Section 2, we present the development of a coupled, two-region model for T_1-T_2 signal prediction by extending the framework for the single-region model presented by Song et al. [12] through the use of an exchange boundary condition at the pore-pore interface [13,14]. The model parameter space is then explored in Section 3 to demonstrate the range of behaviors that might be observed in a T_1-T_2 experiment, including the signal rise behavior noted above. In Section 4, the model is then considered in the context of measurements in three different two-phase/two-region systems. Section 5 synthesizes the results and insights from application of the model to provide some useful guidelines for using the T_1-T_2 sequence in complex settings.

2. Model development

2.1. Setting and assumptions

The model to be developed here addresses the generic problem of the dynamics of diffusion and relaxation in multi-phase, multi-region systems using the ideas first proposed in an NMR context by Brownstein and Tarr [19,20]. By the term *phase*, we mean a portion of a system with distinctly different transport properties (flow, diffusion and reaction, etc.) or NMR properties (relaxation, magnetization, etc.). These distinct properties are homogeneous in character, *i.e.* they occur within the volume of the phase, and so appear as part of the differential balance expressions for the model. For example, a phase might be composed of a porous media (a mixture of fluid and solid materials) and be characterized, through coarse-graining (averaging, smoothing), by an effective diffusion coefficient and effective NMR longitudinal and transverse relaxation times that would appear in the Bloch-Torrey equations [21]. The model of Belton and Hills [14] is an example of two-phase model in which the relaxation and transport properties change across interfaces in a system made up of plant cells or heterogeneous gels.

The term *region*, will identify a portion of the system with distinct length-scale features but not distinct transport or relaxation properties that would characterize a phase. That is, relaxation and transport properties do not change across regions as they would for phases. The two-pore model presented by Zielinski et al. [15] is an example of a two-region system composed of regions with different length scales (a small pore coupled to a large pore) but with the diffusion and relaxation properties that are the same in each of the pores. The random-walk simulations of Song et al. [8] for diffusion and relaxation in porous glass particles is also a two-region model in that it explicitly assumes constant diffusion and relaxation parameters throughout all pore regions.

This study will develop a two-region model; specifically a two-pore model, based on the ideas put forth in Zielinski et al. [15] and incorporating the boundary condition suggested by Belton and Hills [13,14] for inter-region exchange and relaxation processes. Fig. 1 presents the features of single- and two-pore models that we might consider. The single-pore model (Fig. 1a) consists of a pore with a characteristic length scale, L. In the interior of the pore, spins diffuse with diffusion coefficient D, and relax with relaxation rates $R_1 = 1/T_1$ and $R_2 = 1/T_2$. The pore surface, A_s, is impermeable to the spins, but the spins can undergo surface relaxation with surface relaxivity rate coefficient ρ_1 for longitudinal magnetization and ρ_2 for transverse magnetization. Computations for this system will follow the developments of Song et al. [12] and simplify modeling efforts by using one spatial dimension (Fig. 1c).

Features of a two-pore model are shown in Fig. 1b. This system is composed of pores with two distinct pore sizes, L_A, taken as the larger pore and L_B, the smaller pore. The pores are primarily enclosed by surfaces that have the same type of relaxation characteristics as the single-pore model. The pores can have different values for the surface relaxation rate constants, ρ_i, $(i = 1, 2)$ but have the same *homogeneous* relaxation rate constants, $R_i = 1/T_i$ and diffusion coefficients. The pores can be connected (coupled) over the joint areas denoted A_i. The nature of the dynamics on these interfacial surfaces is key to the distinctive character of the two-pore model [13,14].

As was done in the single-pore case, computations for the two-pore model are simplified by using the one-dimensional geometric representation shown in Fig. 1d. In the reduction from the two-and three-dimensional reality of the pore setting to a one-dimensional computational setting, detail is lost. Hence, the specific property

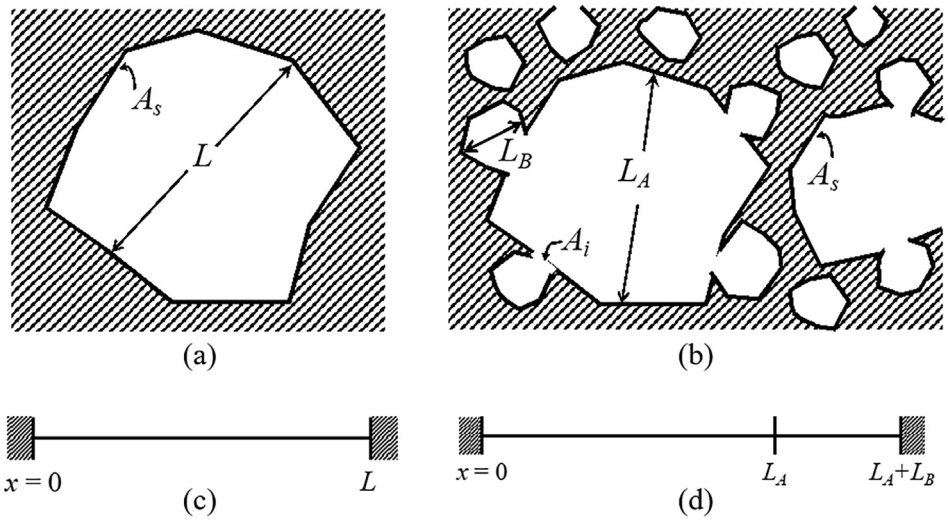

Fig. 1. Settings and geometries for a single-pore (a), (c) and two-pore (b), (d) models.

parameters (using in the one-dimensional version of the two-pore model) should be considered as estimates of intrinsic values.

2.2. The pulse sequence

The aim for developing the model is to simulate the time-domain signal from an NMR pulse sequence. The T_1-T_2 pulse sequence is summarized concisely as [π–t_1–$\pi/2$–t_e–(π–t_e–acq–t_e)$_n$] [3,8]. The duration of the inversion-recovery interval, t_1, following the initial π-pulse is stepped through a series m of logarithmically spaced values and encodes the longitudinal-relaxation characteristics of the material into the signal. At the end of a t_1-interval, a $\frac{\pi}{2}$-pulse generates a time-domain signal from the sample. This signal is acquired as a Carr-Purcell-Meiboom-Gill (CPMG) echo train using a π-pulse separation time of $2t_e$ and consisting of N data points acquired at equal spaced times $t_{2,n} = 2nt_e$, $n = 1, 2, \cdots, N$. This portion of the sequence encodes the transverse-relaxation characteristics of the material into the signal. The net result of the experiment is a two-dimensional array of voltage signals covering the full extent of the t_1 and t_2 values, $s_{m,n} = s(t_{1,m}, t_{2,n})$.

2.3. Governing equations

The goal now is to develop a model that predicts the signal for the experiment. We assume the pulses in the sequence are hard pulses whose time duration is short compared to all other processes of interest in the system. The RF pulses thus set the initial conditions for simulating the evolution of the spin system during the inter-pulse intervals. A predictive model of the system evolution between the pulses is based on the formalism proposed by Song et al. [12] and on the use of the Bloch-Torrey equations [22] to describe the dynamics of diffusion and relaxation processes. The magnetic field within the pores is assumed to be uniform so that dephasing due to diffusion in a non-uniform field caused by susceptibility differences in the sample can be ignored. The Bloch-Torrey (BT) equations for a phase during the inter-pulse intervals then take the form,

$$\frac{\partial M_T}{\partial t} = D\nabla^2 M_T - R_2 M_T \tag{1}$$

for the transverse magnetization and

$$\frac{\partial M_z}{\partial t} = D\nabla^2 M_z - R_1(M_z - M_{\text{eq}}) \tag{2}$$

for the longitudinal magnetization. If we define the generic phase magnetization $m_i = M_{T,i}$ for the transverse magnetization in phase i or $m_i = M_{zi} - M_{\text{eq},i}$ for the longitudinal magnetization for phase i, Eqs. (1) and (2) become

$$\frac{\partial m_i}{\partial t} = D_i\nabla^2 m_i - R_{ij} m_i \;\; i = A, B \;\; j = 1, 2 \tag{3}$$

Eq. (3) encompasses both the Bloch-Torrey equations, which explores the effect of diffusion on evolving magnetization [22], and the Bloch-McConnel equations, which explores the effect of reaction and chemical exchange and relaxation on evolving magnetization [23]. For the Bloch-McConnel equations, $\frac{\partial m_i}{\partial t} = (-R_{i,1} - k_{i,1})(m_i - m_i^0) + k_{j,1}(m_{j,1} - m_{j,1}^0)$, where i and j are the pore regions, diffusion is neglected to focus on reaction exchange mechanisms [23] indicated by $k_{i,1}$. This method has been used to robustly quantify exchange occurring in various systems [5,24–26]. However, in this work, we focus on the diffusion equation parameters and assume a homogenous and diagonalized bulk relaxation.

This two-phase formulation provides direction for a more detailed model but the focus of the present study is to develop a two-pore, *i.e.*, a two *region*, model. The regions share common values of the diffusivity ($D_i \to D$) and relaxation rates ($R_{ij} \to R_j$). These simplifications permit the elimination of the homogeneous relaxation term from Eq. (3) by using the transformation $m_i = u_i e^{-R_j t}$ to obtain

$$\frac{\partial u_i}{\partial t} = D\nabla^2 u_i \quad i = A, B \tag{4}$$

From this result, we note two important items. First, the diffusion equations in Eq. (5) take the same mathematical form for both longitudinal and transverse components and so a common solution process for simulating the pulse sequence will be effective. Second, the homogeneous relaxation processes will not play any role in the interpretation of the final results as they have been "factored out" of the solution.

As shown in Fig. 1, the surface area of the pores in a two-pore system can be divided into separate categories each requiring potentially different boundary conditions (B.C.'s) to characterize them: areas over which there is relaxation of the magnetization at the fluid-solid surfaces (A_s) and areas across which the pores are connected (A_i). At the fluid-solid interfaces, the rate of surface relaxation is matched by the flux of magnetization to those surfaces

$$\boldsymbol{n} \cdot D\nabla u_i|_{A_s} = -\rho_{ij} u_i\Big|_{A_s} \;\; i = A, B \;\; j = 1, 2 \tag{5}$$

where ρ_{ij} is the surface relaxation rate constant for relaxation time mode j (longitudinal relaxation time mode $j = 1$, transverse relaxation time mode $j = 2$), at a fluid-solid surface in pore region i. At the pore-pore boundaries, two B.C.'s are needed since both u_A and u_B are present. Assuming these interfaces do not accumulate magnetization leads to the condition

$$\boldsymbol{n} \cdot D\nabla u_A|_{A_i} = \boldsymbol{n} \cdot D\nabla u_B|_{A_i} \tag{6}$$

Though retained in the expression, the diffusion coefficient plays no role in this boundary condition. The second B.C.'s at the pore-pore interfaces expresses the mechanism of inter-pore transport as

$$\boldsymbol{n} \cdot D\nabla u_A|_{A_i} = k_c(u_B - u_A)|_{A_i} \tag{7}$$

where k_c is a interface conductance, *i.e.*, $1/k_c$ is a interface resistance, which controls exchange of magnetization between regions, analogous to the membrane permeability used by Belton and Hills [13,14].

In the limit as $k_c \to \infty$, the pore-pore interface offers no resistance to the exchange of magnetization and Eq. (7) reduces to an expression of the continuity of magnetization $u_B|_{A_i} = u_A|_{A_i}$ on those interfaces. In the limit as $k_c \to 0$, the boundary is impermeable and Eq. (7) reduces to separate no-flux conditions, one for each region (*i.e.*, $\boldsymbol{n} \cdot \nabla u_A|_{A_i} = 0$ *and* $\boldsymbol{n} \cdot \nabla u_B|_{Ai} = 0$). Depending on the exact nature of the interface, this no-flux condition might not be an appropriate limiting behavior. For example, Zielinski et al. [15] added a relaxation term to the inter-pore boundary condition in the development of their model. As a result, when $k_c \to 0$ in their model, these portions of the pore surfaces would still act as relaxation sinks for magnetization in the pores with the potential for a different rate of relaxation than the fluid-solid surfaces of the pores. To allow for flexibility in handling these limiting behaviors and provide a physically consistent model with respect to the connection between pores, we follow Zielinski et al. [15] and add a surface-relaxation term to B.C.'s at the pore interfaces (Eq. (7)). Hence, at the surfaces A_i, we will use the conditions

$$\boldsymbol{n}\cdot D\nabla u_A|_{A_i} - \rho_{c,Aj}u_A|_{A_i} = \boldsymbol{n}\cdot D\nabla u_B|_{A_i} - \rho_{c,Bj}u_B|_{A_i} \tag{8a}$$

$$\boldsymbol{n}\cdot D\nabla u_A|_{A_i} - \rho_{c,Aj}u_A|_{A_i} = k_c(u_B - u_A)|_{A_i} \tag{8b}$$

where $\rho_{c,ij}, i = A, B$, and $j = 1, 2$ are relaxation rate constants specific to interfacial areas between pores.

2.4. Scaling and solution

The one-dimensional Cartesian version of the diffusion equation with the geometric parameters given in Fig. 1d will be the basis of the solutions we present. L_A is used as a length scale for the model, $t_D = L_A^2/D$ is used as the time scale, and M_{eq} is used to scale magnetizations. The key dimensionless parameters in the model are then the region-size ratio ($\beta = L_B/L_A$), the surface-relaxation Damköhler numbers of the second kind [27] ($\delta_{i,j} = \rho_{i,j}L_A/D$), the interface-relaxation Damköhler numbers ($\delta_{c,ij} = \rho_{c,ij}L_A/D$), and the scaled inter-pore transfer coefficient ($\kappa_c = k_cL_A/D$).

There are 6 parameters in the model and that number can be reduced by connecting the interface-relaxation to the corresponding surface-relaxation through

$$\delta_{c,ij} = \frac{\delta_{i,j}}{1+\kappa_c} \tag{9}$$

This relation provides useful limiting physical behaviors. As $\kappa_c \to 0$, $\delta_{c,ij} \to \delta_{i,j}$ so that when the pores are not connected, all pore surfaces are surfaces with the same relaxation characteristics. As $\kappa_c \to \infty$, $\delta_{c,ij} \to 0$ so that when the regions are fully connected, there is neither interface resistance nor interface relaxation at these boundaries. Hence, the boundary conditions serve to enforce the continuity of magnetization and magnetization flux at the interface between the regions and the system becomes a single-pore system with length $(1+\beta)$. Clearly other relations between $\delta_{i,j}$ and $\delta_{c,ij}$ could be proposed but the expression above is simple, reduces the number of parameters in the model, and provides useful limiting behavior for our model of a two-pore system.

The full model for diffusion and relaxation during an inter-pulse interval is summarized in Appendix A. Here, we provide the essential features of the solution needed for the discussion to come. The solution for the scaled magnetization components has the form

$$u(z,\tau) = u_A(z,\tau) + u_B(z,\tau) = \sum_{k=1}^{\infty} a_k e^{-\lambda_k\tau}\phi_k(z) \tag{10}$$

The key computational problem involves finding the eigensystem of the problem, $\{\lambda_k, \phi_k(z)\}$, consisting of the eigenvalues (λ_k) and their associated eigenfunctions ($\phi_k(z)$).

The eigenvalues will lead to the observed/effective relaxation rates due to the interaction of diffusion and surface relaxation within a pore characterized by the Damköhler numbers $\delta_{i,j}$, and inter-pore exchange of magnetization, characterized by the inter-pore exchange coefficient, κ_c. Each portion of the T_1-T_2 pulse sequence will have its own eigensystem and so, we will refer to the T_1 eigensystem for the dynamics during the inversion-recovery portion and the T_2 eigensystem for the dynamics of the spin-echo portions.

2.5. Pulse-sequence simulation

Using the solutions and eigensystems outlined in Appendix A, the signal from the T_1-T_2 sequence can be predicted following the framework provided by Song et al. [8]. Appendix B provides details of the development and here we summarize the key portions of that simulation. During the inversion-recovery interval, the magnetization evolves according to

$$u(z,\tau) = \sum\nolimits_m a_m^{(1)} e^{-\lambda_m^{(1)}\tau}\phi_m^{(1)}(z) \quad 0 < \tau < \tau_1 \tag{11}$$

where $\tau_1 = t_1/t_D$ is the scaled duration of the T_1 evolution interval. With the state of the system at the end of the τ_1 interval, $u(z,\tau_1)$, providing initial conditions, the system evolves during the spin-echo interval according to

$$u(z,\tau) = \sum\nolimits_n a_n^{(2)} e^{-\lambda_n^{(2)}(\tau-\tau_1)}\phi_n^{(2)}(z) \quad (\tau > \tau_1) \tag{12}$$

The signal for the experiment is acquired during this interval and, using $h(z)$ to represent the coil response function [28], the final expression for the signal is (Appendix B, Eq. (B.7)),

$$\begin{aligned} S(\tau_1,\tau_2) &= \textstyle\sum_{n=1}^{\infty}\sum_{m=1}^{\infty} p_m^{(1)} G_{mn} h_n^{(2)} e^{-r_m^{(1)}\tau_1} e^{-r_n^{(2)}\tau_2} \\ &= \textstyle\sum_{n=1}^{\infty}\sum_{n=1}^{\infty} P_{mn} e^{-r_m^{(1)}\tau_1} e^{-r_n^{(2)}\tau_2} \end{aligned} \tag{13}$$

where $r_k^{(i)} = r_i + \lambda_k^{(i)}$ are the observed relaxation rates. This form of the signal clearly shows that an ILT will recover the amplitudes P_{mn} of the two-dimensional relaxation spectrum of the system.

The amplitudes P_{mn} in Eq. (13) are composed of three factors. The first $p_m^{(1)}$ is the projection of the initial magnetization onto the T_1 eigensystem while the third factor $h_n^{(2)}$ is proportional to the projection of the coil response function [28] onto the T_2 eigensystem. The second factor $G_{mn} = \frac{\langle\phi_m^{(1)},\phi_n^{(2)}\rangle}{\langle\phi_n^{(2)},\phi_n^{(2)}\rangle}$, has been termed the "overlap integral" by Song et al. [7]. It represents the mixing of the two eigensystems, *i.e.* G_{mn} measures the projection of the m^{th} T_1 eigenfunction onto the n^{th} T_2 eigenfunction. As has been discussed extensively in the literature [7,8,10,29], the P_{mn} coefficients in Eq. (13) are not necessarily all positive, a fact that presents challenges for current ILT numerical routines.

The T_1-T_2 time domain signal rise with τ_1 is most clearly observed by scaling the signal in Eq. (13) by the initial value of the magnetization and plotting the reconstituted signal $S(\tau_1,\tau_2)/S(0,\tau_2)$ as a function of τ_1 for different values of τ_2 [8]. This scaling process removes primary relaxation effects due to homogeneous T_1 and T_2 processes and allows us to focus on differential effects of the inter-pore interactions. While the normalization signal $S(0,\tau_2)$ is easily obtained from Eq. (13), experimentally this quantity must be estimated from the shortest values of τ_1 available in a measurement.

3. Model features and predictions

In this section, we explore the parameter space of the model to gain insights into the physics of the system and identify regions where the anomalous signal rise most commonly occurs. Detailed analyses of the eigenfunctions, 2D ILT spectra and time domain signals are provided for two cases: one where the signal rise does occur and one where the rise does not occur. Our aim is to use these base cases to provide physical insights into what information the T_1-T_2 experiment can provide with respect to the molecular dynamics in systems where the rise effect has been observed.

3.1. Model phase space

There are six dimensionless parameters to work with: four Damköhler numbers, $\delta_{i,1}$, $\delta_{i,2}$, $i = A, B$, the inter-pore exchange parameter, κ_c, and pore-size ratio, β. The solution space is potentially quite large and so our approach to understanding the physics of the model is to first explore relaxation-contrast effects and then investigate the effects of exchange and pore-size ratio. Note that the use of the interface/pore-surface relaxation relation (Eq. (9)) eliminates the the need to provide explicit values of $\delta_{ci,j}$.

The Damköhler numbers, $\delta_{i,j}$, represent the ratio of the rate of surface relaxation to the rate of diffusion in pore i for relaxation

mode T_j. When $\delta_{i,j} \ll 1$, pore i is referred to as being in the fast diffusion regime [19]. In the fast-diffusion limit, diffusion acts to maintain an essentially uniform level of magnetization throughout the pore and so the first eigenmode dominates the solution expression (Eq. (10)) for a pore. In this regime, the system response is essentially mono-exponential. When $\delta_{i,j} \gg 10$, the pore is referred to as being in the slow diffusion regime [19]. In the slow-diffusion limit, significant gradients develop in the pores and the interaction of diffusion and relaxation is more complicated. The net result is that the effects of higher order eigenmodes come in to produce a multi-exponential system response [19].

Each of the pores ($i = A, B$) will have two relaxation modes at its surfaces, corresponding to longitudinal relaxation characterized by $\delta_{i,1}$ and transverse relaxation characterized by $\delta_{i,2}$. To manage the complexity of possible relaxation combinations amongst pores, we use a two-element labelling system to characterize the diffusion state of a pore. The first element of the label will refer to the T_1 relaxation mode ($\delta_{i,1}$) and the second label the T_2 relaxation mode ($\delta_{i,2}$) since a pore could be in a fast or slow regime for each of the relaxation modes. For example, we will identify a pore as being fast/slow when $\delta_{i,1} \ll 1$ and $\delta_{i,2} \gg 10$. Similar considerations apply to labeling a pore as fast/fast or slow/slow. The slow/fast mode combination would require $\rho_{i,1} > \rho_{i,2}$ for a pore, a condition which violates the premise that NMR longitudinal relaxation rates should be less than or equal to transverse rates.

The result of this consideration is that each pore can be in one of three conditions (fast/fast, fast/slow, and slow/slow) so there are nine possible ways to combine the labels for two pores. Exploring these combinations, it was found that the condition where the A pore is in the fast/slow regime and the B pore is in the slow/slow regime produced the most significant rise effects. In contrast, the combination of the same modes for both pores, i.e. slow/slow regime for pore A combined with the same the slow/slow or fast/-fast regime for pore B did not show substantial (or any) rise effects.

Fig. 2 summarizes the range of behaviors that were found for this combination of regimes for the A and B pores. The specific parameter values used in the computations are provided in the figure caption. From the figure, we observe the following:

- As $\delta_{A,1}$ increases (Fig. 2a) from 10^{-3} to a maximum of 10^{3}, equivalent to $\delta_{A,2}$ (all other parameters fixed), the A pore moves from having mixed T_1/T_2 modes of fast/slow to being a pore with slow/slow mode. The transition is largely complete once $\delta_{A,1} > 10$ and is not present when $\delta_{A,1} > \delta_{B,1}$. The reduction in the signal rise suggests that strong contrast in pore relaxation mode physics is an important factor leading to signal rise.
- As $\delta_{B,1}$ decreases (Fig. 2b) from 10^{3} (all other parameters fixed), the B pore moves from being a slow/slow pore to a fast/slow pore. For the transition, there is only a relatively small range of values of $\delta_{B,1}$ that lead to a rise in the signal. Further increases in $\delta_{B,1}$ (ending at $\delta_{A,1}$) make the B pore similar to the A pore and that combination of conditions does not lead to signal increase. This result supports the observation noted for Fig. 2a that a strong inter-pore relaxation contrast is needed for a rise to occur.
- Varying the parameter κ_c (Fig. 2c) over a range from 10^{-3} to 10^{3} shows that for small values the system consists of uncoupled or separate pores while at large values the system consists of an effective single pore made up to the two fully coupled pores. The effect of inter-pore exchange on signal rise shown here makes it clear that a rise occurs for intermediate values of κ_c. At the extremes, inter-pore exchange removes any relaxation contrast between the pores which is not conducive to significant signal rises.

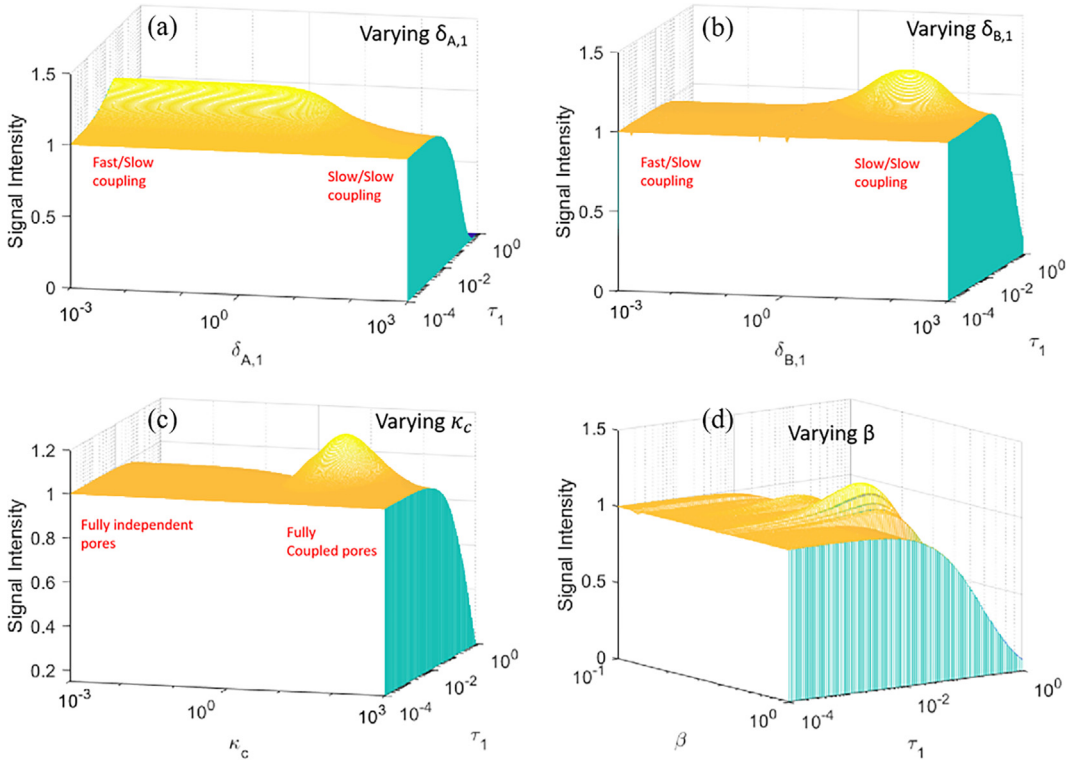

Fig. 2. Parameter phase spaces for $\delta_{A,1}$ (a), $\delta_{B,1}$ (b), κ_c(c) and β (d) are shown. The total time domain signal at $\tau_2 = 2$ is shown. Unless varied, all parameters were kept constant as $\delta_{A,1} = 0.001, \delta_{A,2} = 1000, \delta_{B,1} = 100, \delta_{B,2} = 1000, \beta = 0.33$ and $\kappa_c = 10$. Substantial signal increase appears when the A pore is in fast/slow regime (a) and the B pore is in the slow/slow regime (b). (c) The exchange rate must be intermediate between being too restricted ($\kappa_c \ll 1$, separate pores) and too connected ($\kappa_c \gg 1$, single pore) for significant increases in signals. The geometry of the system, governed by β (d), shows multiple pore ratios for which the increase is seen with no increases occurring at small ($\beta < 0.1$) or large ($\beta > 1$) values.

- The parameter β (Fig. 2d) should range over $0 < \beta < 1$ characterizing the change from a system with one pore ($\beta = 0$) where no signal rise is expected to a two-pore system of equal-sized pores ($\beta = 1$). The transition is not as smooth as those shown in Fig. 2a and b. We do not presently have a clear reason for this lack of smoothness and further analysis is required to resolve this issue. However, it is clear that signal increases occur for $0.25 < \beta < 0.5$ for the given parameter set. Given the physical relevancy of the model [9,11,21,28] the value $\beta = 0.33$ is chosen for detailed analysis going forward.

The primary insights, then, from Fig. 2 are that the conditions that favor substantial signal rise include a strong contrast in the cross-pore longitudinal relaxation parameters ($\delta_{A,1} \gg \delta_{B,1}$) and an intermediate value of the inter-pore exchange rate, κ_c. Viewing the scaled exchange rate as a ratio of characteristic times or rates, $\kappa_c = \frac{k_c L_A}{D} = \frac{L_A^2/D}{L_A/k_c} = \frac{t_D}{t_{ex}} = \frac{\tau_{ex}}{\tau_D}$, it is clear that the exchange rate should be fast (an order of magnitude factor of 10, appears to be the case here) compared to the diffusion rate for the system to ensure that the relaxation-contrast between the pores is able to generate a signal rise. However, too high of an exchange rate reduces the relaxivity contrast between pores and dampens or eliminates any potential for a signal rise.

3.2. Eigensystems, spectra, and time-domain signal features

With a general idea of the conditions which lead to a rise in the time domain signal, we now look into the mechanisms for signal rise by comparing the details of two base cases considered in Fig. 2 (the slow/slow (A), slow/slow (B) and fast/slow (A), slow/slow (B)). The first case to consider is when both pores are in the slow diffusion regime (i.e., $\delta_{A,1}, \delta_{A,2}, \delta_{B,1}$, and $\delta_{B2} > 10$). Fig. 3 summarizes the computational results for this slow/slow setting in the A and B pores.

The first four eigenvalue/eigenfunction pairs are shown in Fig. 3a and demonstrate the discontinuous nature of the eigenfunctions at the interface due to a finite rate of transfer of magnetization there. Higher-order eigenfunctions oscillate with increasing frequency as expected from the nature of the eigenvalue problem. Additionally, the first eigenfunction, as the last one to decay to zero in the solution (based on Eq. (10)), is a useful indicator of the magnetization profile in the system. Due to the large values of the Damköhler numbers, the magnetization at the pore ends are nearly zero and there are significant gradients in each of the pores as a result.

Fig. 3b summarizes the same information for the T_2 eigensystem. There is substantial similarity to the T_1 eigensystem (Fig. 3a) because of the similar Damköhler numbers in this case.

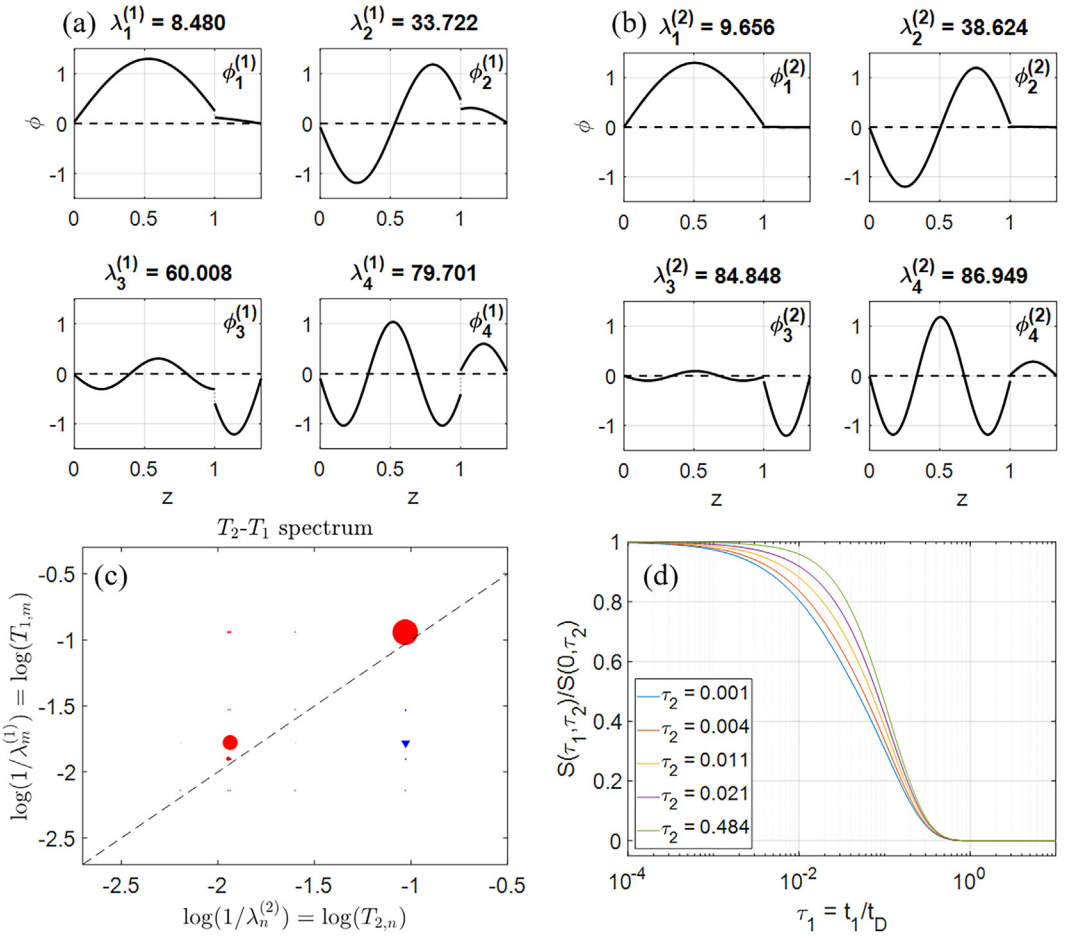

Fig. 3. Results for eigensystem and signals using a base case with coupling between identical slow diffusion modes in two pores for the parameter set $\beta = 0.33$, $\delta_{A,1} = 100$, $\delta_{A,2} = 1000$, $\delta_{B,1} = 100$, $\delta_{B,2} = 1000$, and $\kappa_c = 10$. First four (a) longitudinal eigenfunctions, (b) transverse eigenfunctions and (c) the computed spectrum (P_{mn} values). In (c) blue triangles indicate negative P_{mn} values and red circles indicate positive values. The size of a marker indicates the magnitude of the value. The computed signal for the system is shown in (d). No anomalous rise in time domain signal is observed for this combination of relaxation modes. (For interpretation of the references to colour in this figure legend, the reader is referred to the web version of this article.)

Fig. 3c provides the predicted relaxation-time spectrum. Note that there are minor negative modes as well as modes below the $T_1 = T_2$ diagonal of the spectrum. Finally, Fig. 3d shows the reconstituted time domain signal. There is no signal rise in this case due to the positioning of the dominant relaxation modes above and along the $T_1 = T_2$ diagonal..

The example in Fig. 3 provides a fuller understanding of the elements of the solution to the model. Recall from Eq. (13) that the signal is a weighted sum of exponential terms. The weights are the mode amplitudes, P_{mn}, which comprise three key factors ($p_m^{(1)}$, G_{mn}, and $h_n^{(2)}$) whose values are summarized in Table 1 for $m = n = 4$ terms in the two eigensystems.

The values of $p_m^{(1)}$ are the generalized Fourier expansion coefficients in the expansion of the initial magnetization in terms of the T_1 eigensystem. From the eigenfunctions in Fig. 3a and the values of $p_m^{(1)}$ in Table 1, we see that the value of $p_3^{(1)}$ is important in the reconstruction of the initial condition due to the way that the third eigenfunction provides signal in the B pore relative to the A pore compared to first eigenfunction.

The matrix of the eigenfunction overlap integral G_{mn} values is strongly diagonal, reflecting the similarities of the relaxation aspects of the two eigensystems. Finally, the values of $h_n^{(2)}$ are proportional to the generalized Fourier expansion coefficients in the expansion of the coil response function in terms of the T_2 eigensystem. The specific values of $h_n^{(2)}$in this case arise from the logic that lead to the $p_m^{(1)}$ values: modes with some spatially symmetric character are weighted most heavily in the synthesis of the (constant, symmetric) coil-response function, $h(z)$.

Table 1
Values of the elements of the first four mode amplitudes in Fig. 3c.

m	$p_m^{(1)}$	G_{mn} n				$h_n^{(2)}$	P_{mn} n			
		1	2	3	4		1	2	3	4
1	0.996	1.029	0.055	−0.024	−0.040	0.627	0.642	0.000	0.005	0.007
2	0.078	−0.082	1.002	−0.095	−0.092	0.001	−0.004	0.000	0.002	0.001
3	−0.981	0.100	0.390	1.083	0.270	−0.207	−0.061	−0.000	0.219	0.061
4	−0.151	0.033	0.064	−0.123	0.892	−0.168	−0.003	−0.000	−0.004	−0.023

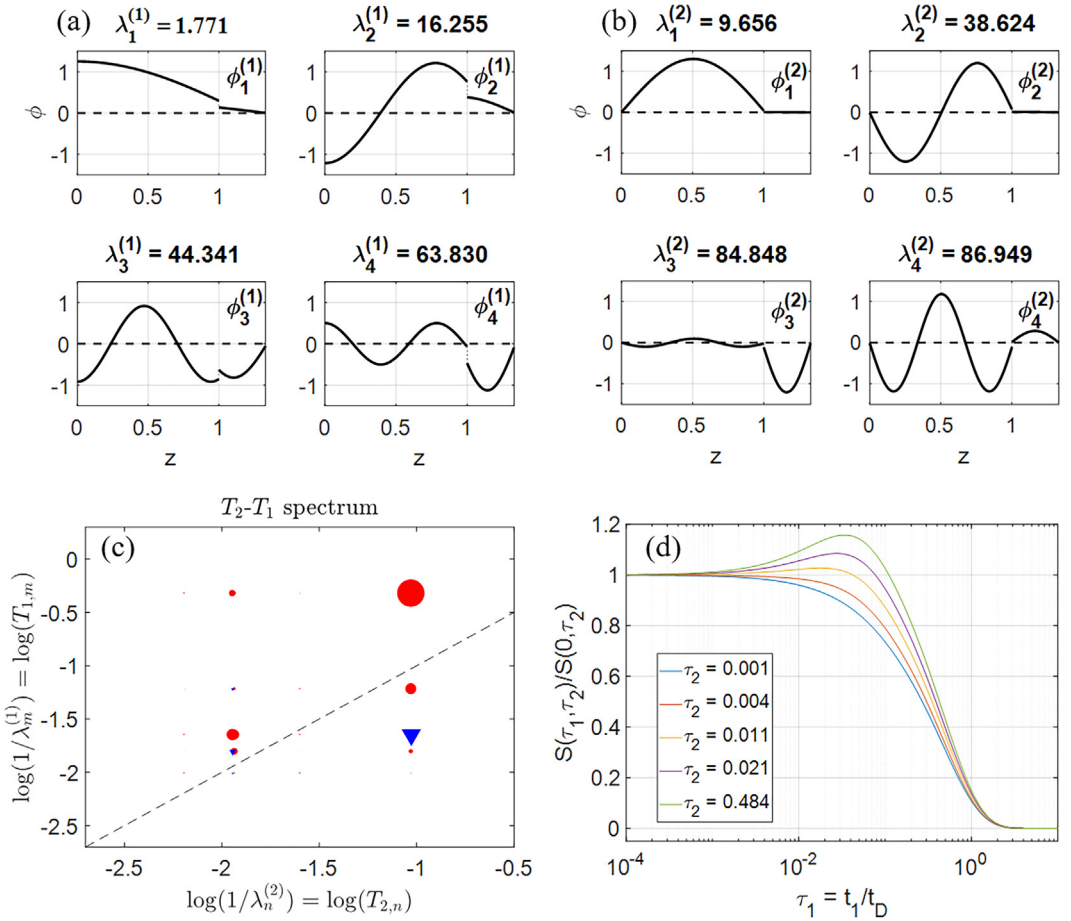

Fig. 4. Results for eigensystem and signals using a base case with coupling between fast and slow diffusion modes in two pores for the parameter set = 0.33, $\delta_{A,1} = 0.001$,$\delta_{A,2} = 1000$, $\delta_{B,1} = 100$, $\delta_{B,2} = 1000$, and $\kappa_c = 10$. First four (a) longitudinal eigenfunctions, (b) transverse eigenfunctions and (c) the computed spectrum (P_{mn} values). In (c) blue triangles indicate negative P_{mn} values and red circles indicate positive values. The size of a marker indicates the magnitude of the value. The computed signal for the system is shown in (d). An anomalous rise in time domain signal is observed for this combination of relaxation modes. (For interpretation of the references to colour in this figure legend, the reader is referred to the web version of this article.)

Fig. 4 repeats the elements of Fig. 3 for the case where the *A* pore is in the fast/slow mode and the *B* pore is in the slow/slow mode. The T_1 eigensystem (Fig. 4a) has changed from the previous case (Fig. 3a) while the T_2 eigensystem is unchanged. The reduction in the Damköhler number $\delta_{A,1}$ in the *A* pore has led to a smaller first eigenvalue and a magnetization profile (using the first eigenfunction as a guide) with gentler gradients but less strong symmetry, a result that will have important consequences in the discussion below.

The time domain signal for this case (Fig. 4d) shows the rise behavior with a magnitude that increases with τ_2. The spectrum (Fig. 4c) is similar to that of the prior case (Fig. 3c) but there are important differences. The negative P_{31} mode amplitude (below the diagonal) is much stronger compared to the dominant P_{11} mode in this case. Table 2, below, summarizes the numerical details using the first four T_1 and T_2 eigenfunctions following the structure of Table 1.

With the change in the spatial characteristics of the first T_1 eigenfunction in pore A (compare Figs. 3a and 4a), more of the $p_m^{(1)}$ terms are needed to synthesize the (constant) initial condition. Importantly, though reduced in magnitude relative to the first, the value of $p_3^{(1)}$ remains negative and that negative value ultimately translates to the negative eigenmode amplitude at P_{31}. The overlap value associated with this negative-going mode, G_{31}, has increased substantially over the value for the slow/slow (*A*) slow/slow (*B*) case (Table 1) due to the decrease in similarity between the two eigensystems. The net result is a stronger negative mode amplitude for P_{31}.

The contrasts between the results in Figs. 3 and 4 amplify the insights into the cause of a rise in the signal that were found in Fig. 2. Specifically, the key requirements for a signal rise are first a strong contrast in the relaxation characteristics between the two pores (compare the first eigenfunctions in Figs. 3 and 4) and second an inter-pore exchange rate that is larger than the diffusion rate ($\kappa_c > 1$) and intermediate to the pore T_1 relaxation rates ($\delta_{A1} < \kappa_c < \delta_{B1}$).

3.3. Time domain signal increase

Observations of anomalous time domain signal increase results in T_1-T_2 measurements of Thrane et al., Williamson et al., and Nelson et al. [16–18] are additional motivation for development of the exchange model. As shown in Fig. 4, the two-region model predicts such a rise in the T_1-T_2 signal, thus providing a tool for investigating the physics that underlie the effects.

The spectra in Fig. 3c and 4c suggest that the interaction of the dominant mode, P_{11}, with the primary negative mode, P_{31}, is key to the development of an increase in the time domain signal amplitude. Because the P_{31} mode means that the short-lived third T_1 mode is coupled to the longest-lived first T_2 mode, a stronger negative value for the P_{31} mode means that the signal as a function of τ_1 will involve a component that decays early in a T_1 sense yet lasts longer in a T_2 sense. Such a setting could lead to a signal rise [9].

A demonstration of how this type of coupling can lead to the observed rise behavior is shown in Fig. 5. Fig. 5a presents the signal components from the case shown in Fig. 3 (no rise observed) while

Table 2
Values of the elements of the first four mode amplitudes in Fig. 4c.

m,n	$p_m^{(1)}$	G_{mn} n				$h_n^{(2)}$	P_{mn} n			
		1	2	3	4		1	2	3	4
1	1.018	0.921	−0.230	−0.033	−0.235	0.627	0.588	−0.000	0.007	0.040
2	0.370	−0.410	0.888	−0.085	0.119	0.001	−0.223	0.000	0.074	0.128
3	−0.446	0.797	−0.440	0.799	1.704	−0.207	−0.223	0.000	0.074	0.128
4	−0.549	−0.044	0.243	0.319	−0.315	−0.168	0.015	−0.000	−0.036	−0.029

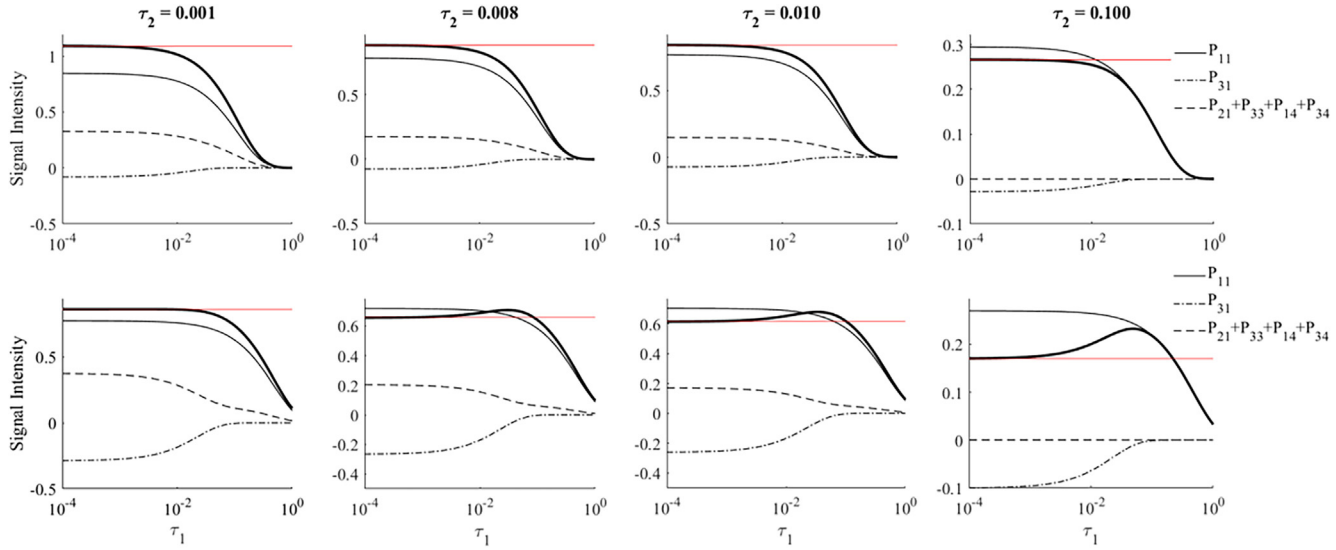

Fig. 5. Demonstration of the contribution of the P_{mn} components to the time domain signal increase for a T_1-T_2 experiment. Lines show the evolution of the signals according to Eq. (14) from the six dominant modes identified from Figs. 3c and 4(c) along with their sum (heavy black line) with the four smallest positive modes combined for clarity. The thin (red) solid line locates the value of the sum as $\tau_2 \to 0$ and helps to identify the rise in the signal with increasing τ_1. (a) Shows the slow/slow mode coupling case of Fig. 3 and (b) the fast/slow mode coupling of Fig. 4 for increasing τ_2 or echo number. (For interpretation of the references to colour in this figure legend, the reader is referred to the web version of this article.)

Fig. 5b does the same for the signal in Fig. 4 (rise observed). The time evolution of six significant modes from those figures all take the form

$$f_m(\tau_1;\tau_{2n}) = P_{mn}e^{-\lambda_m^{(1)}\tau_1}e^{-\lambda_n^{(2)}\tau_{2n}} \quad (14)$$

for a given set of τ_{2n} values.

At short values of τ_2, there is little differential T_2 weighting of the modes, and all modes contribute in proportion to their P_{mn} value to the observed signal. In Fig. 5, the relative strength of the P_{11} mode, along with the smaller positive modes (P_{33}, P_{34}, P_{13}, and P_{14}) add together to balance out any effect of the negative P_{31} mode might have on the signal. However, by $\tau_2 = 0.1$, most of the smaller, higher-eigenvalue modes have decayed to zero leaving only the P_{11} and P_{31} modes, modes that are associated with the longest T_2 mode. If the magnitude of the P_{31} is much smaller than the dominant P_{11} mode (as it is in Fig. 3), the increase in the signal due to the decay of this negative model is not of importance and as the total signal drops to zero without a rise in the τ_1 dimension (Fig. 5a). When P_{31} is larger (Fig. 4), however, the decay of the mode makes a noticeable addition to the signal i.e., a signal rise is observed.

From this discussion, though negative mode amplitudes are necessary for generating a rise in the T_1-T_2 time-domain signal, it is clear that they are not sufficient for the rise to appear. For example, negative modes are part of the system shown in Fig. 3 but the magnitudes of those modes are not large enough to cause the offsets shown in Fig. 4. In such cases, the T_1-T_2 signal is spread out in the τ_1 domain as a function of the particular τ_2 value. Also, if the largest negative mode has a decay rate that is closer to the dominant positive mode decay rate, the rise in the signal could actually appear as a spread in the T_1-T_2 signal decay as τ_1 increases.

4. Experimental observations

The increase in the time domain signal for T_1-T_2 experiments was first reported by Song et al. [8] for a microporous glass bead system. Diffusive coupling between the internal microscale pores within the beads and macroscale pores due to bead packing was shown to generate an increase in the reconditioned time domain signal [8]. An increase in the T_1-T_2 time domain signal was also observed for a polymer/solvent (HPMCAS/acetone) system in a weak gel state above the glass transition temperature [17] and in the formation of hydrates of agglomerates of hydrate cages [16]. Here data for the microporous glass bead system, the cyclopentane/water hydrate system and beeswax undergoing a solid-solid rotator phase transition [18] are presented. The data is discussed in the context of using the exchange model to demonstrate the insight into measurements of complex systems that is possible. The model as investigated here is most directly applicable only to the microporous beads. Extension to include bulk relaxation heterogeneity is necessary to further quantify the dynamics in the other systems.

4.1. Microporous bead pack

The data of Song et al. [8] was reproduced using the same 150 μm microporous beads (CPG2000A, Millipore) in a water-saturated bead pack. A 2 MHz Rock Core Analyzer (Magritek Ltd, Wellington NZ) was used to acquire T_1-T_2 correlation data. The T_1 domain was sampled with 32 logarithmically spaced values of τ_1 from 1 to 1000 ms and a CPMG readout train with a τ = 800 μs pulse spacing and 1500 echoes. The data is shown in Fig. 6 and clearly indicates a signal rise in the t_1 domain with increases in t_2. The results here are also in accord with those of Song et al. with signal maxima occurring around $t_1 \sim 0.01$ s and the onset of the growth of the rise in the signal appearing at about 320 ms.

In addition to particle size, Song et al. [8] provide material characteristics that can provide estimates of the parameters for the two-pore model presented here. The total porosity of the system was reported as $\epsilon = 0.8$. The pore volume of the system was equally apportioned between the interior and exterior of the beads. Using the reported external porosity of $\epsilon_e = 0.4$, the interior porosity of the particles is calculated to be $\epsilon_i = 0.67$. The internal length scale of the beads was reported as $l_i = 0.3$ μm.

Our initial analysis will assume pore A is represented by the water external to the beads. To establish a length scale, L_A, we use a unit cell of width l_e that contains a layer of thickness l_p representing the water-saturated bead. Hence, for the interval $l_p < x < l_e$, there is only water. From geometric considerations and the equal apportioning of water between the regions in the system, we have that $\frac{\epsilon_p V_p}{V_e - V_p} = \frac{\epsilon_p l_p}{l_e - l_p} = 1$ which implies $l_e = (1+\epsilon_p)l_p = (5/3)l_p$. Hence, with l_p approximately the particle radius, the length-scale for the region A is given as $L_A = l_e - l_p = \varepsilon_p l_p = (2/3)l_p \approx 50$ μm. From this length scale and the diffusion coefficient of water

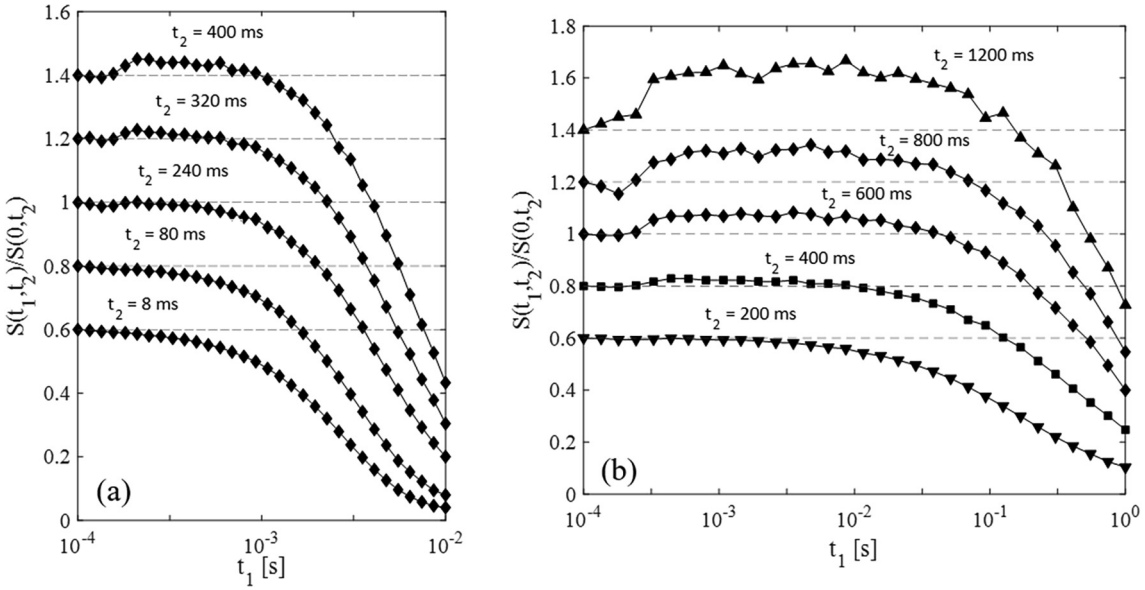

Fig. 6. T_1-T_2 time domain signal for 150 μm microporous bead pack in water at 2 MHz. The signal rise is detected at 320 ms and grows through the end of the CPMG train.

($D = 2.5 \times 10^3$ μm^2/s), the time scale for the system is estimated to be $t_D = L_A^2/D \sim 1$ s. A similar computation using spheres rather than flat layers to represent the phases leads to $t_D \sim 0.16$ s and we infer a reasonable estimate of the diffusion time to be in the range of these values. Measurements by Song et al. of surface relaxation rates (at 2 MHz) suggest that ρ_1 and ρ_2 are on the order of 1 and 10 μm/s, respectively, leading to the guideline that $\frac{\delta_{A,2}}{\delta_{A,1}} = \frac{\rho_1}{\rho_2} \sim 10$. From the scaling information so far, the initial estimates of the Damköhler numbers are $\delta_{A,1} \sim 0.01$ and $\delta_{A,2} \sim 0.1$ indicating a fast longitudinal diffusion mode and a fast to intermediate transverse diffusion mode.

Identifying the *B* pore with the micropores in the beads leads to the finding that $L_B \sim 0.31$ μm, and so $\beta \sim 10^{-2}$. As was made clear from the discussion of Fig. 2d, we would not expect a substantial rise to occur for this pore-size ratio. Thus, our approach, will be to find a value of β that produces a rise and use that value to indicate an effective size of the *B* pore relative to the *A* pore. With regard to Damköhler numbers for the *B* pore, Song et al. [8] suggest that the internal relaxation rates for the internal bead micropores will be much higher than the external rates due to the small micropore length scale. We anticipate that both homogeneous relaxation in pore *B* along with $\delta_{B,1}$ and $\delta_{B,2}$ is greater than the values in the *A* pore to provide the slow/slow conditions needed to generate the rise behavior. This argument suggests a second *phase* as we have defined for this model rather than two simple regions. More on both of these issues will be provided in the discussion to follow.

Based on these considerations, a range of model parameter combinations was explored in an effort to capture the trends in the data shown in Fig. 6. The results are summarized in Fig. 7. To be clear, the comparison here is not an optimized fit of the model to the data. Rather, the parameters were chosen (see the caption for Fig. 7 for specifics) to be consistent with the data, the parameters provided by Song et al., and with the criteria we have developed for what conditions do and do not lead to predictions of a rise in the reconstituted signal for the experiment.

As is evident from Fig. 7, a reasonable fit of the model to measurements is possible, especially for the t_1 interval for which the rise develops. Given the level of estimation of the parameters involved, we find the correspondence shown here to be quite encouraging as it strongly suggests that pore-pore interactions are key to the anomalous rise behavior in this system.

There are, however, some important discrepancies between the model and the data. The model misses the long-t_1 behavior in the data at any value of t_2. Further analysis and experimentation with other model systems will be required to get insight into the reason for this discrepancy. One possibility is that the system is actually best described by a three region-model (Region 1: external water between particles, Region 2: internal water in "large pores", Region 3: internal water in "small pores"). A light coupling between Region 1 and the other regions would leave the spins in Region 1 largely unimpacted by interactions with the solid and hence would lead to a portion of the system with longer relaxation times. This alternative view of the system would also imply that the model predictions in Fig. 7 are associated with the material heterogeneity or the microstructure of the beads themselves. Indeed, such a revised conception of the system would also help make sense of the value of $\beta = 0.4$ used in the computations and suggest that the "larger" pores are about 2–3 times as large as the "smaller" pores. Though these extensions to the model are outside the scope of the current study, they could provide the basis for further work on the model and its application.

Finally, the comparison in Fig. 7 also involves an inflation of the scaled times in the t_2 dimension that is 100 times greater than that of the required diffusion-time-scale inflation (i.e., $t_2 = 100 t_D \tau_2$ for the curves shown). We do not have a clear idea of why such a rescaling is needed. Part of the issue might be related to the ideas mentioned above for the t_1 axis but the order of magnitude of this rescaling seems to be much too large for an addition of a non-interacting region. The large values of the Damköhler numbers ($\gg$10) could also be a part of the issue since these values are key to establishing the observed relaxation times in this system. However, rise behavior in the current model depends on the fast/slow behavior of a pore and so reducing the values of $\delta_{i,2}$ in order to increase the predicted lifetime of the spins would eliminate the prediction of the observed effect. We leave this issue unresolved and look to further work in this area to provide insights.

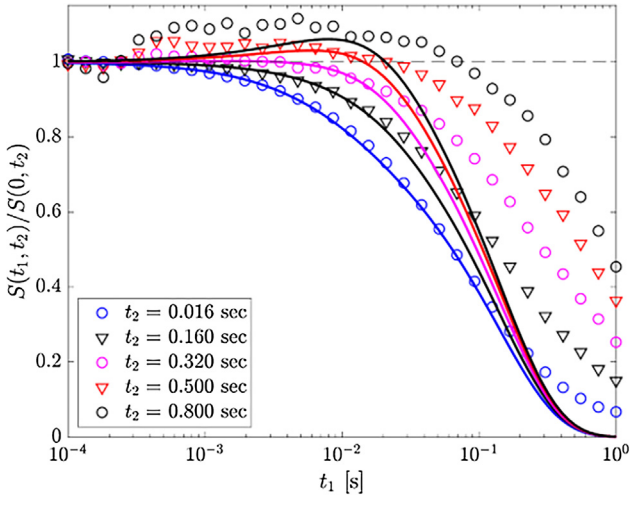

Fig. 7. Comparison of the two-pore model (solid lines) with the microporous bead data of Fig. 6 (symbols). Model parameter values were $L_A = 20$ μm, $D = 2500$ μm^2/s, $\delta_{A1} = 0.01$, $\delta_{A2} = 100$, $\delta_{B1} = 100$, $\delta_{B2} = 1000$, $\kappa_c = 10$, and $\beta = 0.4$. Values of $S(0, t_2)$ were estimated from the first 5 t_1 values at any given t_2 value in the signal array, s (*t*1,m, *t*2,n). The time scale used for the $t_1 = t_D \tau_1$ dimensional axis of the model is the diffusion time for the experimental spherical particle system ($t_D = 0.16$ s). The dimensional time-scale for the model t_2 curves was increased by a factor of 100 over the diffusion time $t_2 = 100 t_D \tau_2$ to provide the registration of the data and model as shown.

4.2. Organic hydrate formation – cyclopentane/water

During the formation of hydrates, a porous hydrate shell consisting of hydrate cage agglomerates will form around thawing ice particles dispersed in the organic cyclopentane phase [16]. The exchange between the regions of high mobility excess cyclopentane and the cyclopentane entrained in the porous structure formed by the hydrate agglomerate generates a time domain T_1-T_2 signal increase due to the coupling of the diffusion dynamics, see Fig. 8. The structure of the hydrate cage agglomerate porous media evolves from a porosity of ~95%, when hydrate formation begins, to 5% over the hydrate formation time [16,30]. The hydrate system exhibits complex diffusion dynamics on the mesoscale of the agglomeration of hydrate cage structures as shown by the signal increase with t_1. On the scale of microseconds and Angstroms, water molecules cage one single cyclopentane molecule and the cages agglomerate to form structure III hydrates [31]. The rise in the time domain signal is from the coupling of the bulk pentane and pore scale pentane, an analogous system to the microporous bead pack [8]. To apply the model to this system, the porosity of the hydrate shell would be represented by the model pore connectivity term κ. However due to the evolution of the hydrate shell the model would need to be extended to allow a time dependent pore connectivity. Appropriate choice of model parameters to capture the diffusion dynamics during hydrate formation is further complicated by the magnetization loss from water and cyclopentane

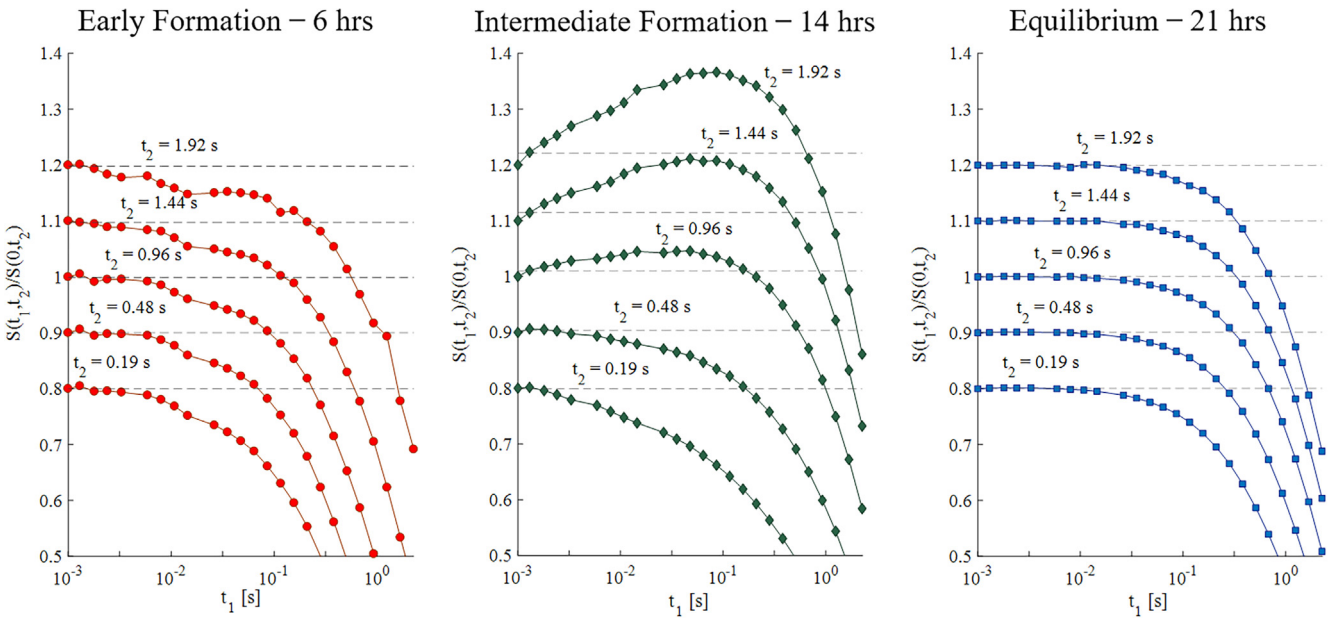

Fig. 8. T_1-T_2 time domain signal for a model hydrate forming system of water and excess cyclopentane. The signal rise indicates diffusive coupling between bulk cyclopentane and cyclopentane in micron size pores of agglomerates of hydrate cages. At early times (6 h) the agglomerate is of very low porosity and does not impact the signal. After hydrate formation is complete, the signal rise is not present as the very high density $\phi < 5\%$ of the porous structure effectively prevents exchange through the hydrate shell.

molecules which are not detectable once entrained in the hydrate cage structure. The T_1-T_2 time domain signal rise occurs at intermediate ~14 h formation times, but not at early times when the high porosity of the porous agglomerate does not significantly impact cyclopentane diffusion and relaxation, nor interestingly at long time equilibrium after all water is consumed. Studies with anti-agglomerate chemicals, which keep the cages in a nanoparticle slurry state, showed no signal increase [16].

4.3. Multi-component wax – beeswax

Beeswax, a mixture of long chain alkanes, esters with smaller amounts of free acids and alcohols, exhibits a polymorphic crystalline structure at room temperature [32]. Solid-solid phase transitions occur throughout heating, breaking the conformation of the polymorphic lattice and introducing mobility into the system. These transitions occur at temperatures from 36.4 °C up to the beginning of the softening point at 50.0 °C which is due to the transition from a crystalline state to an intermediate state [32]. The softening of the lipid matrix has been characterized through ^{13}C ssNMR [32–35] and is described as a transition from a dominated *trans* configuration with short T_2 with small populations of *gauche* structures of longer T_2, to the shift toward a primarily *gauche* lattice. This initial breaking of the symmetry toward a *gauche* structure is captured by the T_1-T_2 measurements shown in Fig. 9. Unlike the microporous bead pack and the hydrate sys-

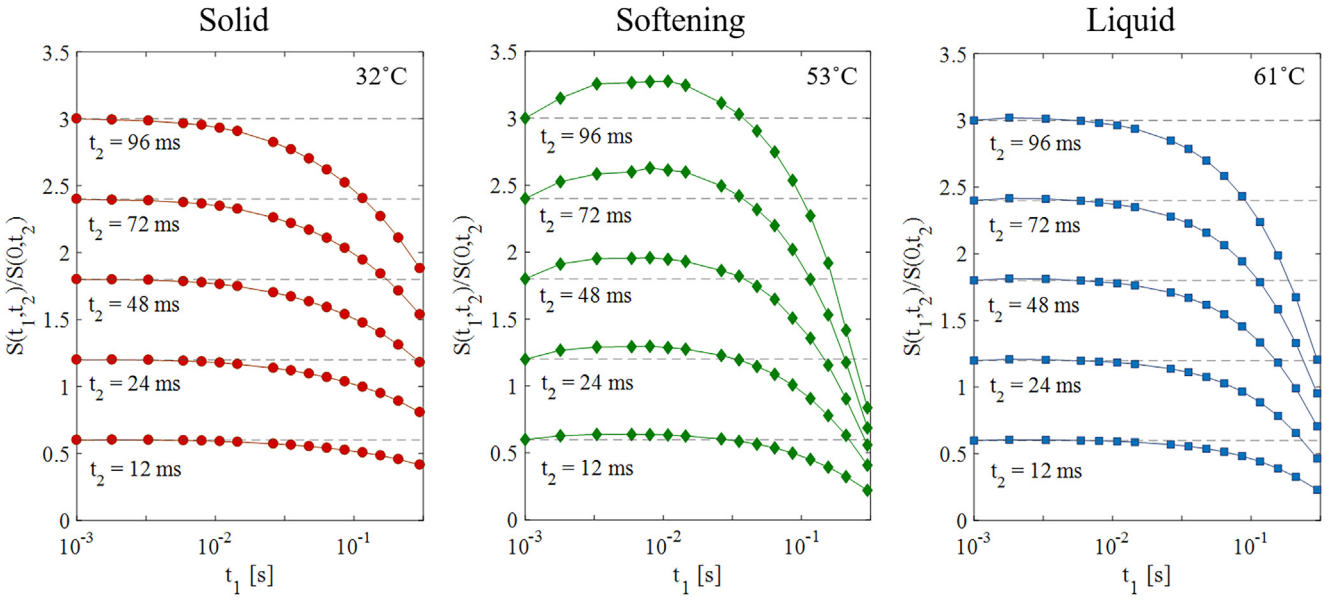

Fig. 9. T_1-T_2 time domain signal for beeswax, a complex wax, is shown. The signal rise is not present in the crystalline solid state at 32 °C, nor at the homogenous liquid state at 61 °C. In the softening state at 53 °C, the signal rise indicates exchange occurring which is not brought on through mass transfer. Rather spin diffusion is the mechanism of exchange causing the anomalous time domain signal rise.

tem, this system does not have mass transfer occurring. It provides an example of the observed time domain signal increase as a function of physico-chemical state due to flip- flop spin diffusion [35] between the *trans* and *gauche* domains [18]. Spin diffusion ssNMR measurements use double quantum, or other RF filters, to selectively excite regions of strong dipolar coupling and use diffusion models to quantify spin diffusion between crystalline and amorphous domains [36]. The spin diffusion model of Buda et al. [36] posits an interfacial domain between the crystal domain magnetization source and amorphous domain magnetization sink, through which the magnetization diffuses. Their model is analogous to that introduced here, with $\kappa_c = D_I/d_I$, where D_I is the flip-flop spin diffusivity of the interface which occurs through a thickness d_I, without surface relaxation effects.

5. Conclusions

Song et al. [8] demonstrated an increase with experimental time τ_1 in the reconditioned time domain signal in T_1-T_2 correlation experiment. In this paper the observation of an increase in the time domain signal from T_1-T_2 correlation experiments is demonstrated to depend on exchange of magnetization between domains of different surface relaxivity in a simple 1D diffusion and relaxation model [14,19]. The model indicates that the presence of negative eigenmodes is necessary to induce a signal increase in the time domain. However, the negative modes must also be of sufficient amplitude. The negative value of the eigenmode can come from the projection of the initial condition onto the third T_1 eigenfunctions, from the coil response function projected on the first T_2 eigenfunctions and the eigenfunction overlap or correlation between the third longitudinal and first transverse eigenfunctions. It is the amplitude of overlap and its rate of change with τ_1 that generates the time domain signal rise. This provides novel insight into the specific origin in the coupled diffusion problem and the role of negative eigenmodes on T_1-T_2 measurements [7,10,12,15].

The signal rise effect on the time domain T_1-T_2 signal provides a robust means to determine coupling or exchange between regions of different diffusion and relaxation behavior. Experimental examples of the signal increase have been demonstrated in a microporous glass bead packed beds [8], where coupling between large and small pores due to molecular diffusion is present. In a high concentration polymer-solvent system [17], where molecular diffusion exchange between solid and liquid like domains of a glassy state is present and in hydrate formation where organic phase cyclopentane diffuses through an evolving porous structure of agglomerated hydrate [16]. These systems are consistent with the model developed in terms of varying fast and slow diffusion modes among domains and mass transport mediated magnetization exchange. The signal rise effect is also shown for a solid-solid phase transition in a complex lipid system, beeswax, where no mass transport between different domains occurs [18]. Further analysis of the underlying physics mechanisms generating this effect in the context of the model presented here and other extensions could provide a robust time domain method for the characterization of magnetization exchange in complex systems.

Acknowledgements

Yi-Qiao Song for providing the sample of the porous glass material. JEM was provided support through sabbatical funding from Bucknell University. JDS and SLC thank the M.J. Murdock Charitable Trust for equipment funding and Bend Research Inc. a Lonza Company for partial research funding.

Appendix A. Solution to the coupled, two-pore model

A one-dimensional, Cartesian version of the diffusion equation is used for computations of magnetization dynamics in a pore. The problem is scaled in order to simplify the notation and bring out the key dimensionless parameters [37]. Scaling position by the size of the larger pore, L_A, time by the diffusion time, L_A^2/D, magnetization by M_{eq}, and factoring out the homogeneous relaxation terms, we arrive at the dimensionless version of the two-pore problem, Eq. (4), with boundary conditions given by Eqs. (5) and (8) as

$$\frac{\partial u_A}{\partial \tau} = \frac{\partial^2 u_A}{\partial z^2} \tag{A.1a}$$

$$u_A(z,0) = u_{A0}(z) \tag{A.1b}$$

$$-\left.\frac{\partial u_A}{\partial z}\right|_0 = -\delta_A u_A(0,\tau) \tag{A.1c}$$

$$\left.\frac{\partial u_A}{\partial z}\right|_1 + \delta_{cA} u_A(1,\tau) = \left.\frac{\partial u_B}{\partial z}\right|_1 - \delta_{cB} u_B(1,\tau) \tag{A.1d}$$

$$\left.\frac{\partial u_A}{\partial z}\right|_1 = \kappa_c(u_B(1,\tau) - u_A(1,\tau)) \tag{A.1e}$$

$$\left.\frac{\partial u_B}{\partial z}\right|_{1+\beta} = -\delta_B u_B(1+\beta,\tau) \tag{A.1f}$$

$$u_B(z,0) = u_{B0}(z) \tag{A.1g}$$

$$\frac{\partial u_B}{\partial \tau} = \frac{\partial^2 u_B}{\partial z^2} \tag{A.1h}$$

This problem statement holds for both the longitudinal and the transverse magnetization components. Computations presented in Section 3 will use the relation between the Damköhler numbers at the pore-pore interface and the pore-surface Damköhler numbers given in Eq. (9) to eliminate the need to specify the δ_{ci}-values separately from the δ_i-values.

A normal-modes method can be applied to solve the coupled-pore diffusion problem given in Eqs. (A.1) [12]. The approach posits that the solution for the interval $0 < z < (1+\beta)$ takes the form

$$u(z,\tau) = \sum_{k=1}^{\infty} a_k e^{-\lambda_k \tau} \phi_k(z) \tag{A.2}$$

where the elements of the eigensystem $\{\lambda_k, \phi_k(z)\}$ are λ_k, the eigenvalues, and $\phi_k(z)$, the eigenfunctions. Note the eigenfunctions are *composites* of two distinct separate component eigenfunctions that separately cover each of the pores, *A* and *B*, i.e. $\phi_k(z) = \phi_{A,k}(z) + \phi_{B,k}(z)$, where $\phi_{A,k}$ is defined for $0 < z < 1$ and $\phi_{B,k}$ is defined for $1 < z < \beta$. The coupling boundary conditions, Eqs. (A.1d) and (A.1e), ensure the solution obtained by adding the two component functions is a solution to the problem. Additionally, the inter-pore transfer boundary condition in Eq. (A.1e), allows for a discontinuity in the composite eigenfunction at the interface. The component eigenfunctions are continuous outside of the interface.

The elements of the eigensystem for the problem are obtained from the coupled set of ordinary differential equations extracted from the spatial portions of the model, Eqs. (A.1).

$$\frac{d^2\phi_{A,k}}{dz^2} + \lambda_k \phi_{A,k} = 0 \quad 0 < z < 1 \tag{A.3a}$$

$$\left.\frac{d\phi_{A,k}}{dz}\right|_0 = \delta_A \phi_{A,k}(0) \tag{A.3b}$$

$$\left.\frac{d\phi_{A,k}}{dz}\right|_1 + \delta_{cA}\phi_{A,k}(1) = \left.\frac{d\phi_{B,k}}{dz}\right|_1 - \delta_{cB}\phi_{B,k}(1) \tag{A.3c}$$

$$\left.\frac{d\phi_{A,k}}{dz}\right|_1 + \delta_{cA}\phi_{A,k}(1) = \kappa_c(\phi_{B,k}(1) - \phi_{A,k}(1)) \tag{A.3d}$$

$$\left.\frac{d\phi_{B,k}}{dz}\right|_{1+\beta} = -\delta_B \phi_{B,k}(1+\beta) \tag{A.3e}$$

$$\frac{d^2\phi_{B,k}}{dz^2} + \lambda_k \phi_{B,k} = 0 \quad 1 < z < 1+\beta \tag{A.3f}$$

The eigenfunctions for different eigenvalues are orthogonal on the interval $[0, (1+\beta)]$ ([38,39]) as quantified by the inner product

$$\begin{aligned}\langle \phi_m, \phi_n \rangle &= \int_0^{1+\beta} \phi_m(z)\phi_n(z)dz \\ &= \int_0^1 \phi_{A,m}(z)\phi_{A,n}(z)dz + \int_1^{1+\beta} \phi_{B,m}(z)\phi_{B,n}(z)dz \\ &= 0 \quad m \neq n\end{aligned} \tag{A.4}$$

Any initial conditions for the problem (Eqs. (A.1b) and (A.1g)) can be used to provide the constants a_k in the solution (Eq. (A.2)) as $a_k = \frac{\langle u_0, \phi_k \rangle}{\langle \phi_k, \phi_k \rangle}$ with $u_0(z) = u_{A0}(z) + u_{B0}(z)$ as the (composite) initial condition.

The problem presented in Eqs. (A.3) is linear and is it is possible to obtain analytical expressions for the eigenfunctions [14]. However, there is substantial algebraic complexity to finding the eigenvalues for the general case which precludes finding simple, closed-form expressions for the eigenvalues. For eigensystem computations presented in this study, solutions to Eqs. (A.3) were found using MATLAB™ and the CHEBFUN toolbox [40].

To obtain the code used for the eigensystem computations and system simulation, please contact the author, James E. Maneval, Bucknell University, maneval@bucknell.edu.

Appendix B. Details of the development of the signal for the T_1-T_2 pulse sequence

The system is assumed to be at equilibrium before the start of the pulse sequence so that $M_z(z,0) = M_{eq}$. The initial π-pulse inverts the magnetization to form the initial condition for the first interval as $M_z(z,0) = -M_{eq}$. Setting $m = M_z - M_{eq}$ for the inversion-recovery interval gives $m(z,0) = -2M_{eq}$ and, in terms of u, this initial condition is $u(z,0) = -2$. The eigensystem in this interval is the T_1 eigensystem, $\{\lambda_m^{(1)}, \phi_m^{(1)}\}$, and is computed using the longitudinal relaxation parameters, δ_{i1} and δ_{ci1} along with the parameters κ_c and β. The system evolves according to,

$$u(z,\tau) = \sum\nolimits_m a_m^{(1)} e^{-\lambda_m^{(1)}\tau}\phi_m^{(1)}(z) \quad 0 < \tau < \tau_1 \tag{B.1}$$

with $\tau_1 = t_1/t_D$ as the scaled duration of the T_1 evolution interval. The coefficients in the expansion above are computed from the T_1 eigensystem by using the initial condition $u(z,0) = -2$ to give

$$a_m^{(1)} = -2\frac{\langle 1, \phi_m^{(1)} \rangle}{\langle \phi_m^{(1)}, \phi_m^{(1)} \rangle} \tag{B.2}$$

The $\frac{\pi}{2}$-pulse then converts the longitudinal magnetization to transverse magnetization to provide the initial condition for the spin-echo portion of the sequence as

$$u(z,\tau_1) = \sum\nolimits_m a_m^{(1)} e^{-\lambda_m^{(1)}\tau_1}\phi_m^{(1)}(z) \tag{B.3}$$

The eigensystem in this second interval is the T_2 eigensystem, $\{\lambda_n^{(2)}, \phi_n^{(2)}\}$, and is computed using the transverse relaxation parameters, $\delta_{i,2}$ and $\delta_{ci,2}$ but with the same values of κ_c and β used for the T_1 eigensystem. With the state of the system at the end of this interval, $u(z,\tau_1)$, providing the initial conditions, the system then evolves during the second, spin-echo interval $\tau > \tau_1$ according to

$$u(z,\tau) = \sum\nolimits_n a_n^{(2)} e^{-\lambda_n^{(2)}(\tau-\tau_1)}\phi_n^{(2)}(z) \quad (\tau > \tau_1) \tag{B.4}$$

The coefficients in Eq. (B.4) are obtained from the initial condition for the interval as

$$a_n^{(2)} = \frac{\langle 1, \phi_n^{(2)} \rangle}{\langle \phi_n^{(2)}, \phi_n^{(2)} \rangle} - 2e^{-r_1\tau_1}\sum\nolimits_m \frac{\langle 1, \phi_n^{(1)} \rangle}{\langle \phi_n^{(1)}, \phi_n^{(1)} \rangle}\frac{\langle \phi_m^{(1)}, \phi_n^{(2)} \rangle}{\langle \phi_n^{(2)}, \phi_n^{(2)} \rangle} e^{-\lambda_m^{(1)}\tau_1} \tag{B.5}$$

Note the coefficients for this solution involve the details of the T_1 eigensystem results as well as the duration of the inversion-recovery interval, τ_1 due to the initial condition for the solution in the second interval that is set by the final condition of the inversion-recovery interval (Eq. (B.3)).

The signal during the post- $\frac{\pi}{2}$ pulse is obtained by integration over the whole system, weighted by the coil-response function $h(z)$. Using the solution for the spin-echo interval, we have the signal for the experiment as,

$$\begin{aligned}s(\tau_1,\tau_2) &= e^{-r_2\tau_2}\int_0^{1+\beta} u(z,\tau_2)h(z)dz \\ &= e^{-r_2\tau_2}\sum\nolimits_n a_n^{(2)} h_n^{(2)} e^{-\lambda_n^{(2)}\tau_2}\end{aligned} \tag{B.6}$$

with $h_n^{(2)} = \int_0^{1+\beta} h(z)\phi_n^{(2)}(z)dz$ proportional to the projection of the response function onto the T_2 eigensystem and $\tau_2 = \tau - \tau_1$ is the (scaled) time for signal acquisition during the CPMG decay. Simplifications in the expression are possible by defining the difference of the final signal based on the equilibrium magnetization [12]. Writing $S(\tau_1,\tau_2) = s(\tau_1 \to \infty, \tau_2) - s(\tau_1,\tau_2)$, Eqs. (B.3)–(B.6) lead to the signal for the experiment as

$$\begin{aligned}S(\tau_1,\tau_2) &= \sum_{n=1}^{\infty}\sum_{m=1}^{\infty}\frac{\langle 1,\phi_m^{(1)}\rangle}{\langle \phi_m^{(1)},\phi_m^{(1)}\rangle}\frac{\langle \phi_m^{(1)},\phi_n^{(2)}\rangle}{\langle \phi_n^{(2)},\phi_n^{(2)}\rangle} h_n^{(2)} e^{-r_m^{(1)}\tau_1}e^{-r_n^{(2)}\tau_2} \\ &= \sum_{n=1}^{\infty}\sum_{m=1}^{\infty} p_m^{(1)} G_{mn} h_n^{(2)} e^{-r_m^{(1)}\tau_1}e^{-r_n^{(2)}\tau_2} \\ &= \sum_{n=1}^{\infty}\sum_{n=1}^{\infty} P_{mn} e^{-r_m^{(1)}\tau_1}e^{-r_n^{(2)}\tau_2}\end{aligned} \tag{B.7}$$

where $r_k^{(i)} = r_i + \lambda_k^{(i)}$ are the observed relaxation rates, combinations of the homogeneous rate constants and the eigenvalues for the problem.

References

[1] Magnetic resonance in porous media: Recent progress. J. Chem. Phys. 128(5) (2008) 052212.
[2] B. Blumich, NMR Imaging of Materials, Clarendon, Oxford, 2002.
[3] P.T. Callaghan, Translational Dynamics and Magnetic Resonance, vol. 1, Oxford University Press, New York, NY, 2011.
[4] J.H. Lee et al., Two-dimensional inverse Laplace transform NMR: altered relaxation times allow detection of exchange correlation, J. Am. Chem. Soc. 115 (17) (1993) 7761–7764.
[5] S.E. Mailhiot et al., Quantifying NMR relaxation correlation and exchange in articular cartilage with time domain analysis, J. Magnet. Reson. 287 (2018) 82–90.
[6] J. Edmund, L.V. Fordham, Jonathan Mitchell, Andrea Valoriz, What are, and what are not Inverse Laplace Transforms, Diffusion Fundam. 29 (2017) 1–8.
[7] D. Bytchenkoff, S. Rodts, Structure of the two-dimensional relaxation spectra seen within the eigenmode perturbation theory and the two-site exchange model, J. Magnet. Reson. 208 (2011) 4–19.
[8] Y.Q. Song et al., Experimental identification of diffusive coupling using 2D NMR, Phys. Rev. Lett. 113 (23) (2014) 235503.
[9] L. Schwartz, D. Johnson, J. Mitchell, T. Chandrasekera, E. Fordham, Modeling two-dimensional magnetic resonance measurements in coupled pore systems, Phys. Rev. E 88 (2013) 032813.
[10] T.C. Chandrasekera, J. Mitchell, Numerical inversion methods for recovering negative amplitudes in two-dimensional nuclear magnetic resonance relaxation-time correlations, Phys. Rev. E 98 (4) (2018) 043308.

[11] R. Song et al., The robust identification of exchange from T2–T2 time-domain features, J. Magn. Reson. 265 (2016) 164–171.
[12] Y.-Q. Song, L. Zielinski, S. Ryu, Two-dimensional NMR of diffusion systems, Phys. Rev. Lett. 100 (2008) 248002.
[13] P.S. Belton, B.P. Hills, E.R. Raimbaud, The effects of morphology and exchange on proton N.M.R. relaxation in agarose gels, Mol. Phys. 63 (5) (1988) 825–842.
[14] P.S. Belton, B.P. Hills, The effects of diffusive exchange in heterogeneous systems on N.M.R. line shapes and relaxation processes, Mol. Phys. 61 (4) (1987) 999–1018.
[15] L. Zielinski, Y.-Q. Song, S. Ryu, P. Sen, Characterization of coupled pore systems from the diffusion eigenspectrum, J. Chem. Phys. 117 (2002) 5361–5365.
[16] L.W. Thrane, J.D. Seymour, S.L. Codd, Probing molecular diffusion during hydrate formation by high-field NMR relaxometry and diffusometry, J. Magnet. Reson. 303 (2019) 7–16.
[17] N.H. Williamson et al., Glass dynamics and domain size in a solvent-polymer weak gel measured by multidimensional magnetic resonance relaxometry and diffusometry, Phys. Rev. Lett. 122 (6) (2019) 068001.
[18] M.L. Nelson, L.W. Thrane, S.L. Codd, J.L. Cape, C.D. Craig, J.D. Seymour, Observing solid-solid phase transitions with NMR relaxometry, Phys. Chem. Chem, Phys, 2019.
[19] K.R. Brownstein, C.E. Tarr, Importance of classical diffusion in NMR studies of water in biological cells, Phys. Rev. A 19 (6) (1979) 2446–2453.
[20] K. Brownstein, C. Tar, Spin-lattice relaxation in a system governed by diffusion, J. Magnet. Reson. 26 (1977) 17–24.
[21] B. Penke, S. Kinsey, S. Gibbs, T. Moerland, B. Locke, Proton diffusion and t1 relaxation in polyacrylamide gels: a unified approach using volume averaging, J. Magnet. Reson. 132 (1998) 240–254.
[22] H. Torrey, Bloch equations with diffusion terms, Phys. Rev. 104 (1956) 563–565.
[23] H.M. McConnell, Reaction rates by nuclear magnetic resonance, J. Chem. Phys. 28 (3) (1958) 430–431.
[24] B. Hills et al., T_1-T_2 correlation analysis of complex foods, Appl. Magn. Reson. 26 (4) (2004) 543–560.
[25] N. Marigheto et al., Methods for peak assignment in low-resolution multidimensional NMR cross-correlation relaxometry, J. Magnet. Reson. 187 (2) (2007) 327–342.
[26] L. Venturi et al., Multidimensional cross-correlation relaxometry of aqueous protein systems, Appl. Magn. Reson. 33 (3) (2008) 213–234.
[27] R.B. Bird, W.E. Stewart, E.N. Lightfoot, Transport Phenomena, second ed., Wiley & Sons, New York, 2002, p. 780.
[28] D.I. Hoult, R.E. Richards, The signal-to-noise ratio of the nuclear magnetic resonance experiment, J. Magnet. Reson. 213 (2) (2011) 329–343.
[29] S. Rodts, D. Bytchenkoff, Structural properties of 2D NMR relaxation spectra of diffusive systems, J. Magnet. Reson. 205 (2010) 315–318.
[30] I. Rao et al., Gas hydrate deposition on a cold surface in water-saturated gas systems, Indust. Eng. Chem. Res. 52 (18) (2013) 6262–6269.
[31] M.R. Walsh et al., Microsecond simulations of spontaneous methane hydrate nucleation and growth, Science 326 (5956) (2009) 1095–1098.
[32] T. Kameda, Y. Tamada, Variable-temperature 13C solid-state NMR study of the molecular structure of honeybee wax and silk, Int. J. Biol. Macromol. 44 (1) (2009) 64–69.
[33] T. Kameda, 13C solid-state NMR analysis of heterogeneous structure of beeswax in native state, J. Phys. D, Appl. Phys. 38 (24) (2005) 4313–4320.
[34] T. Kameda, Molecular structure of crude beeswax studied by solid-state C-13 NMR, J. Insect. Sci. 4 (2004).
[35] A. Abragam, Principles of Nuclear Magnetism, Oxford University Press, USA, 1983.
[36] A. Buda, D.E. Demco, M. Bertmer, B. Blümich, B. Reining, H. Keul, H. Höcker, Domain sizes in heterogeneous polymers by spin diffusion using single-quantum and double-quantum dipolar filters, Solid State Nuclear Magnet. Reson. 24 (1) (2003) 39–67, https://doi.org/10.1016/S0926-2040(03)00020-1.
[37] W.B. Krantz, Scaling Analysis in Modeling Transport and Reaction Processes, John Wiley & Sons Inc., 2007.
[38] D. Ramkrishna, N. Amundson, Transport in composite materials: reduction to a self adjoint formalism, Chem. Eng. Sci. 29 (1974) 1457–1464.
[39] C. Tittle, Boundary value problems in composite media: quasi- orthogonal functions, J. Appl. Phys. 36 (1965) 1486–1488.
[40] L. Trefethen, Approximation Theory and Practice, SIAM, 2013.